Composites: Part A 145 (2021) 106368

Contents lists available at ScienceDirect

Composites Part A

journal homepage: www.elsevier.com/locate/compositesa

Continuous evolution of processing induced residual stresses in composites: An in-situ approach

Sandeep Chava, Sirish Namilae *

Department of Aerospace Engineering, Embry-Riddle Aeronautical University, Daytona Beach, FL 32114, USA

ARTICLE INFO

Keywords:
Residual stresses
Warpage
Composite laminates
Digital Image Correlation (DIC)
Autoclave processing
In-situ monitoring

ABSTRACT

Processing induced residual stresses are often responsible for causing warping, undesired distortion, dimensional instability, and delaminations in composite structures. Monitoring the evolution of residual stresses throughout the cure is essential to understand their effect on the mechanical behavior of the composites. In the present work, a novel in-situ experimental approach is used to measure the dimensional changes in the laminates during cure and combined with temperature-dependent moduli obtained from Dynamic Mechanical Analysis (DMA) to calculate the continuous evolution of residual stresses during composite processing. Five symmetric and asymmetric layup configurations are analyzed to investigate the effect of ply orientation on the residual stress evolution. The maximum average residual stress of 110 MPa in the longitudinal direction is observed for symmetric cross-ply $[0/90]_s$ configuration and the maximum average warpage of 1.46 mm is observed for balanced unsymmetric [30/−30/60/−60] layup configuration.

1. Introduction

Residual stresses which arise during composite manufacturing are self-balanced stresses that exist in the absence of external loads. They typically reduce the mechanical properties of the composite and lead to defects like warpage. Processing induced residual stresses are caused because of the directional properties of plies [1], polymerization shrinkage of the matrix during curing, and due to the dissimilar thermomechanical response of matrix and fibers during thermal cycling [2]. The magnitude of residual stresses is an important consideration in designing load-bearing structures as they cause warping [3], undesired distortion [4], and dimensional instability [5]. They can prestress the structure and affect the overall strength by causing microcracks in the matrix [6], which can lead to further environmental degradation. It is, therefore, necessary to factor in the residual stresses in the processing and design of composite structures.

Researchers have developed a wide range of approaches to measure the residual stresses through destructive and non-destructive experimental methods, as well as modeling techniques. Chapman et al. used the layer removal method by placing separation films within a laminate during cure [7]. Cowley et al. created unsymmetric or unbalanced layups by milling outer plies of the laminate and then measure the resulting changes in curvature [8]. The optical methods such as Moiré interferometry [9] and fiber-optic Bragg gratings [10] have been used for measuring residual stresses in a composite laminate by using a modified hole drilling method. Transverse residual stresses in cross-ply laminates have been estimated using the first ply failure method [11]. In addition to these destructive techniques, non-destructive methods like X-ray diffraction [12], neutron diffraction [13], photoelasticity [14], acoustic waves [15], and Raman spectroscopy [16] have also been used for measuring the residual stresses. However, requirements like crystallinity limit the application of x-ray diffraction and neutron diffraction methods for carbon fiber composites [17]. Ifju et al. used the cure referencing method (CRM) to measure the processing induced strains in laminated composites by incorporating moiré interferometry and replication of diffraction grating on the surface of the laminate during autoclave cure [18]. The residual stresses are then calculated using the laminate theory and strains measured by the Moiré interferometry after cure. Croom et al. used digital image correlation (DIC) as a method for in-situ probing of the residual stresses in air plasma spray (APS) coatings through curvature measurements [19]. DIC has also been used in additive manufacturing to evaluate the effect of build direction on residual stresses in stainless steel specimens [20]. In addition, several modeling methods including energy methods [21], elasticity solution [22], CLT based macro-mechanics approaches [8] and unit cell finite element models [23] have been used to model and predict the residual

* Corresponding author.
E-mail address: Sirish.Namilae@erau.edu (S. Namilae).

https://doi.org/10.1016/j.compositesa.2021.106368
Received 17 September 2020; Received in revised form 27 January 2021; Accepted 27 February 2021
Available online 14 March 2021
1359-835X/

stresses.

Monitoring the evolution of residual stresses throughout the cure cycle will help in developing a deeper understanding of the manufacturing process. This can lead to changes in the manufacturing process that lower the residual stresses and thereby mitigate the associated processing defects and strength-reduction. Most of the studies that measured the residual stresses from the literature are limited to post-cure measurements. In-situ approaches that use sensors like embedded strain gauges and fiber optics introduce a foreign body into the laminate which changes the material properties. Approaches for the evaluation of residual stresses continuously during cure are limited due to the experimental requirements of incorporating the monitoring setup inside an autoclave. The objective of this study is to address these constraints and develop an experimental approach to continuously evaluate the processing induced residual stresses in composite laminates. A non-destructive in-situ method for monitoring processing induced strains was developed by the authors and utilized to study wrinkle formation [24]. That approach is adapted to measure the dimensional changes during curing in this study and is combined with temperature-dependent moduli obtained from Dynamic Mechanical Analysis (DMA) to calculate the continuous evolution of residual stresses during composite processing. Further, the effect of layup configuration on the residual stress evaluation is examined by analyzing and comparing several symmetric and asymmetric layup configurations.

2. In-situ experimental procedure & characterization

Unidirectional carbon fiber prepreg procured from Fibre Glast Corporation containing 12 K tow raw material is pre-impregnated with an epoxy resin system of density 1.2 g/cc and has a fabric areal weight of 139 g/m^2. This prepreg is cured at the manufacturer recommended curing temperature of 120 °C (248F) with a one hour hold time. The specimen temperature is measured using a J-type thermocouple inside the autoclave. The specially designed autoclave from ASC Systems is instrumented with a 3D digital image correlation (DIC) setup as shown in Fig. 1. This autoclave is also equipped with a borosilicate glass viewport and an interior light which enables the DIC measurement as seen in Fig. 1(b). The cameras of the DIC system are set up pointing at the composite layup through the viewport of the autoclave. The VIC-3D Real-Time DIC System from Correlated Solutions measures the surface ply deformations and strains during the composite processing by extracting full-field information from the high contrast random speckle pattern sprayed on the surface ply as seen in Fig. 2 using high-temperature spray paint. Composite specimens of dimensions 101.6 mm × 152.4 mm (4-inch × 6-inch) are prepared for fabrication using four plies of unidirectional carbon fiber prepreg in two symmetric orientations of $[0/90]_s$, $[0/45]_s$, and two unsymmetric orientations of [30/−30/60/−60], [0/30/45/90] and one anti-symmetric orientation of [45/−45/45/−45].

Dynamic mechanical analysis (DMA) using PerkinElmer - DMA 8000 is performed to characterize temperature-dependent dynamic viscoelastic properties of the composite material used in this research. A small unidirectional four-ply sample of dimensions 50 mm × 7.5 mm was mounted using a three-point bending setup to obtain both temperature dependent longitudinal and transverse modulus of the material. Differential scanning calorimetry (DSC) using DSC-3 from Mettler Toledo is performed to measure the degree of cure for the prepreg resin used in this research. Resin samples of weight 25 mg to 35 mg extracted by scraping from the prepreg were placed and sealed in 40 μL aluminum crucibles. The experimental procedure is carried out in two steps, dynamic and isothermal. First, the samples are heated at a constant rate of 10 °C/min between −25 °C to 250 °C (dynamic) and the temperature was held constant at 120 °C (isothermal) for a time of 0 min to 60 min with 10 min intervals. The degree of cure of the sample at these 10 min intervals was calculated and plotted by comparing the isothermal heat of reaction to the total heat of reaction until complete cure.

3. Results and discussion

3.1. Temperature-Dependent elastic properties

The results from the DMA are analyzed during the hold and cool-down phases of the cure cycle. Temperature-dependent Young's modulus ($E_L(T)$ & $E_T(T)$) values are experimentally extracted through the DMA of the sample and are plotted against temperature. The average change in modulus during the cool-down phase for four different samples can be seen in Fig. 3. The rate of change in longitudinal modulus is lower during the initial cool-down phase and then increases to an average of 272 GPa at room temperature. On the other hand, the transverse modulus increases sharply and then gradually levels off towards the end to 7.9 GPa at room temperature. The manufacturer provided tensile modulus for the prepreg is 275.8 GPa [25]. A similar trend of change in modulus is also observed by Li et al. in their theoretical model [26] and the experimental measurements of Kim et al. [27]. The error bars denote the standard deviation from four different samples.

3.2. Cure kinetics

The cure kinetics of the resin was analyzed using the DSC and the degree of cure (DOC) (α) is calculated as the ratio of change in heat of reaction (ΔH_t) and total heat of reaction (ΔH_{total}) as shown in Eq. (1) [28].

$$\alpha(t) = \frac{\Delta H_t}{\Delta H_{total}} = \frac{\Delta H_{total} - \Delta H_R}{\Delta H_{total}} \quad (1)$$

Where, ΔH_R is the residual heat of reaction for the isothermally cured sample at 120 °C for time *(t)*. The total heat of reaction is measured through dynamic scanning test form −25 °C to 250 °C at a predefined heating rate of 10 °C/min as the resin is completely cured. The degree of

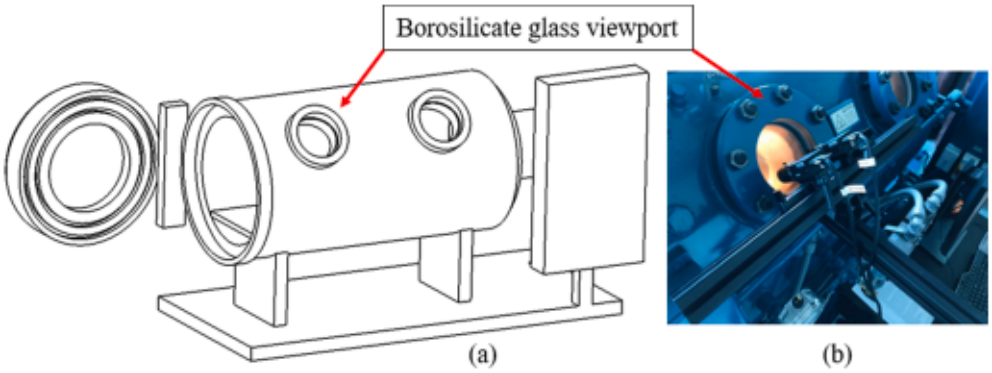

Fig. 1. (a) Schematic of the autoclave with viewports; (b) DIC monitoring setup.

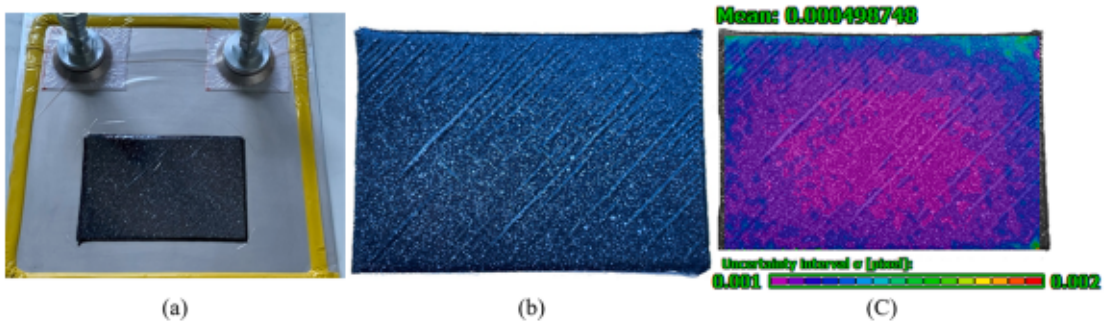

Fig. 2. [45/−45/45/−45] laminate: (a) under vacuum bagging; (b) speckle pattern after cure; (c) DIC uncertainty of speckle pattern.

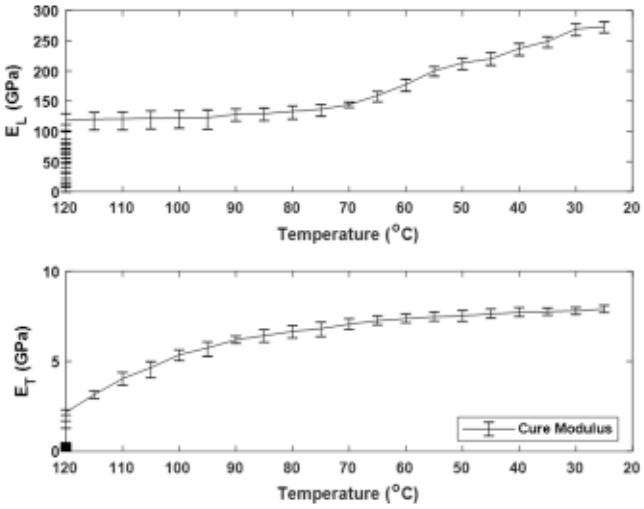

Fig. 3. Change in Young's Modulus (E_L and E_T) to temperature.

cure for the hold-phase and cool-down phase of the cure cycle can be seen in Fig. 4. The ΔH_R after the ramp-up with zero isothermal hold time corresponds to a degree of cure of 20%. Therefore, the B-stage resin in the prepreg is 20% cross-linked as-procured. The epoxy reaches vitrification, the point at which resin is converted from a rubbery state to a glassy state at 70 min. Comparing the mobility in the vitrified state before and after 70 min, the mobility after 70 min is much lower to permit further reaction, hence this point is considered as vitrification point [29]. This corresponds to 94% cross-linking as seen in Fig. 4. The resin is 97% cured at the end of the cure.

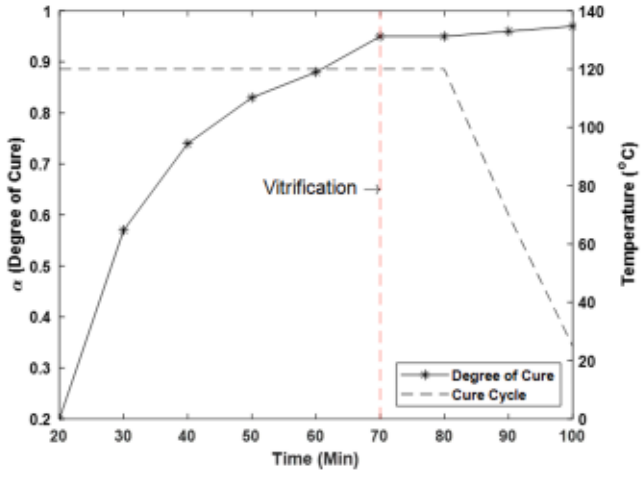

Fig. 4. Degree of cure curve correlated with autoclave cure profile.

3.3. In-situ strain data and analysis

DIC is employed to measure the surface strains of all the layup configurations used in this research. The DIC system used in this work has a minimum in-plane strain measurement capability of 0.005% (50E−6), with a resolution of 10E−6 [30]. The uncertainty in the displacement and strain measurement depends on several factors including focus, lighting, glare, F-stop, subset size, and the speckle pattern quality [31]. For the typical experimental conditions and the speckle pattern used here, VIC 3D software computes a mean uncertainty of about 0.00049 pixels for every pixel as shown in Fig. 2 (c). For the strain measurements in the range of 5E−3, typically observed in this work, this leads to a possible measurement error of around ± 1%.

For a unidirectional single-ply laminate, the average surface strains ($\varepsilon_{unidirectional}$) are correlated with the cure cycle of the composite as shown in Fig. 5 (a). During the ramp-up phase of the cure, the composite expands in both longitudinal and transverse directions, primarily due to the thermal expansion of the matrix and fibers. At this stage, there is no contribution of cure shrinkage. This expansion is higher for transverse than longitudinal direction (3E−3 for T vs 1.7E−3 for L). In the isothermal stage, cure shrinkage and thermal effects are both responsible for the strain. A maximum strain of 3.76E−3 is observed in the transverse direction during the hold-phase at 50 min into the cure. After vitrification and during cool down, the observed contraction is again primarily due to thermal effects. At the end of the cure, it can be seen that the longitudinal strain (1.2E−3) is higher than the transverse strain (2E−4) because the thermal effects are more prominent in the transverse direction both during ramp-up and cool-down. Fig. 5 (b) shows the contour plot of the spatial distribution of the transverse strain at the end of the cure.

The measured surface strains ($\varepsilon_{laminate}$) for the other ply configurations in longitudinal and transverse directions are shown in Figs. 6 and 7 respectively. Although strain measurements using DIC are always on the top ply, the ability of the inner plies to restrict the motion of the top ply can be observed in these figures. Particularly three out of the five layup configurations adopted in this research have 0° ply as top ply but the difference in the evolution of strain throughout the hold phase and cool-down phase among these four layups is evident. Since this paper's focus is on residual stresses, these figures are plotted from the 20 min point to focus on strain and stress build-up from the stress-free point. Also, the reference state of the strain (zero strain) is shifted from the initial state to the stress-free point as the load transfer goes to zero at the stress-free point at the beginning of the isothermal stage and starts again as the cross-linking of the resin begins during the isothermal stage and continues through the cool-down.

In the longitudinal direction, the strain in $[0/90]_s$ layup increases continuously throughout the cure to 0.91E-3 by the end of the cure. A maximum strain of 0.17E-3 is observed for $[0/45]_s$ layup due to the effect of 45° ply in the layup. The strain decreases to −1.0E−3 at the end of the cure. The longitudinal strain development in the unsymmetric layups is shown in the lower half of Fig. 6. A maximum strain of 0.38E−3

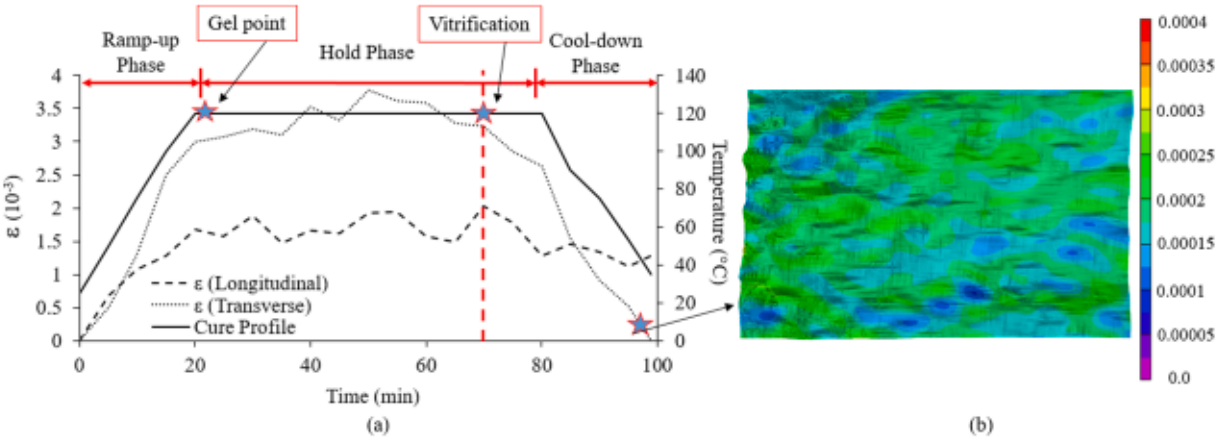

Fig. 5. (a) Unidirectional single-ply average strains; (b) Longitudinal single-ply strain contour at the end of the cure.

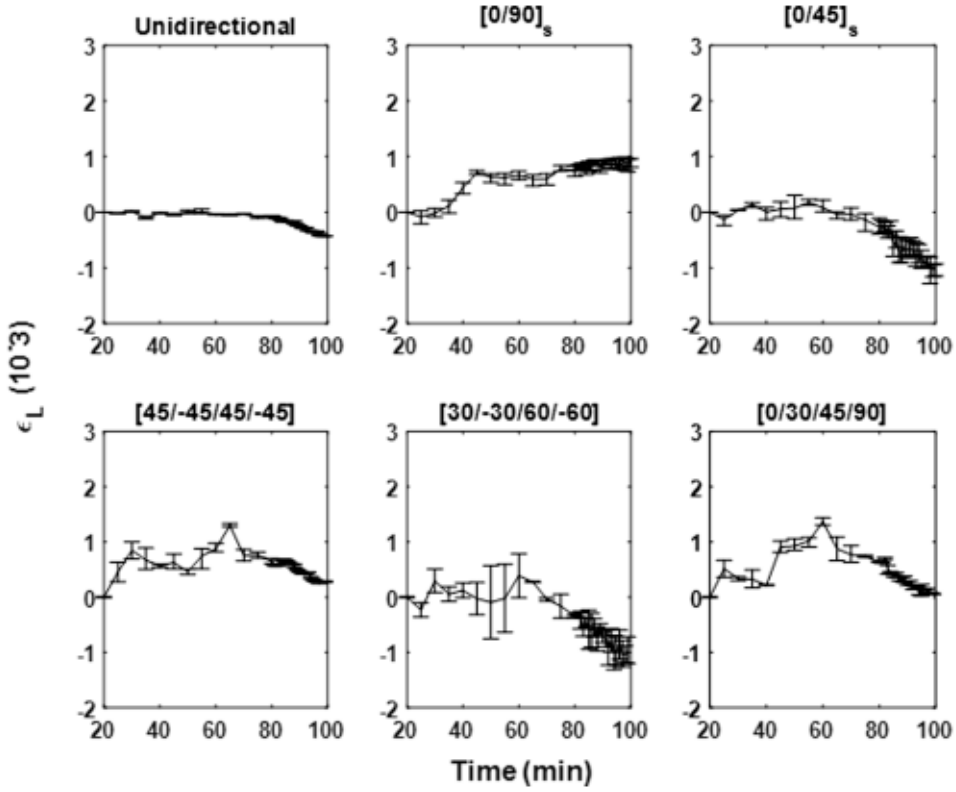

Fig. 6. Laminate strains in the longitudinal direction.

is observed for the [30/-30/60/-60] layup and gradually decreases to −0.96E−3 at the end of the cure due to the balanced nature of the layup. For the unsymmetric [0/30/45/90] layup, the strain increases to a maximum during the hold phase and then slightly decreases to 0.05E-3 at the end.

In the transverse direction, as seen in Fig. 7, for $[0/90]_s$ configuration, a maximum strain of 0.71E-3 is observed and then reduces to −0.13E−3 at the end of the cure. Due to the cross-ply nature of this configuration, the change in strain during cooling is relatively low. In the case of $[0/45]_s$ layup, a maximum strain is observed at the start of the hold-phase and gradually the strain decreases to −1.53E−3 at the end of the cure. For asymmetric layups, [45/−45/45/−45] exhibited negligible changes throughout hold and after cool-down, it reduced to −0.45E−3. Initially, a maximum strain of 0.81E−3 is observed for the [30/−30/60/−60] layup and the strain gradually decrease to −1.39E-3 at the end of the cure due to the balanced nature of the layup. For [0/30/45/90] layup with strain gradually decreasing from 1.05E-3 to −1.68E-3 during the hold and cool-down phases of the cure due to distinct ply orientations.

Although these are surface strain measurements, any significant movement in the interior plies due to thermomechanical loads during cure as well as residual stresses generated due to the crosslinking of the polymer bonds will be reflected on the surface due to the relatively low thickness of the sample.

3.4. Residual stress calculation

Residual stresses within a ply are calculated by using the liberated strain approach. This is the strain difference between what a ply is experiencing during the cure and what the ply would experience if it is not constrained by the neighboring plies. The liberated strain is calculated based on the assumption that strain measured at the surface

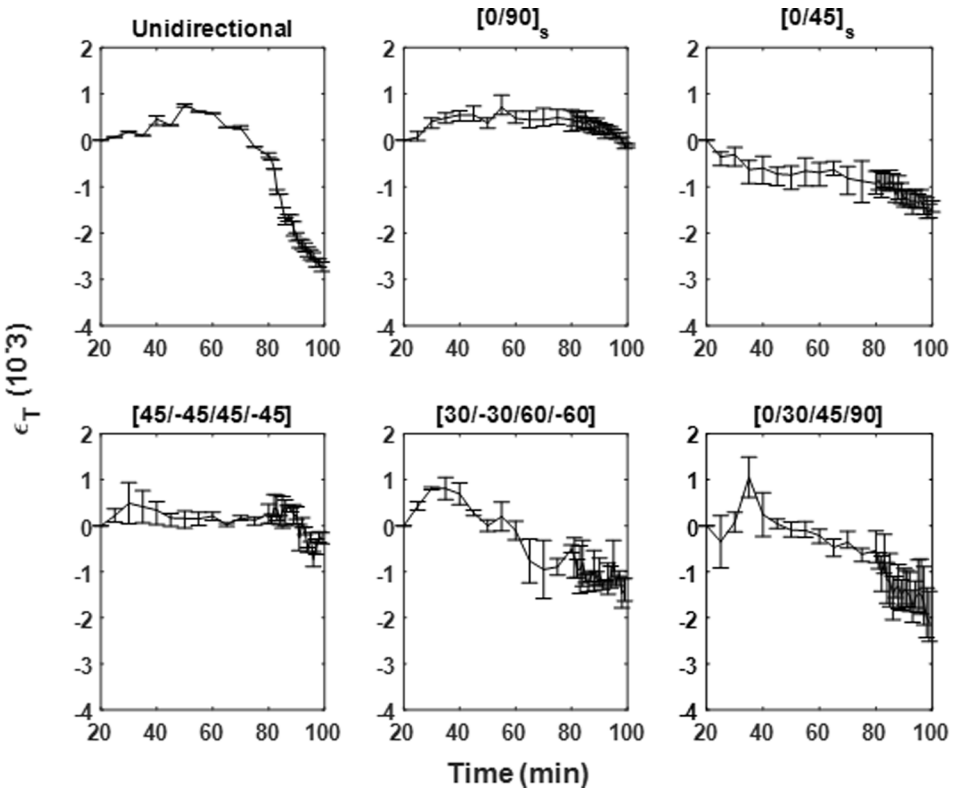

Fig. 7. Laminate strains in the transverse direction.

through DIC matches the strain at any point in the interior of a thin plate. The four-ply laminate configuration adopted in this research is considered to be a thin structure. The residual strain for each ply was calculated as a difference between a ply s unidirectional strain and the strain within a laminate transformed by the transformation matrix $_k$ as shown in Eq. (2). The angle ‘ in Eq. (3) is the angle between the global coordinate x-axis and the direction of the fiber in the considered ply. This residual strain is a function of ply orientation and includes the thermal expansion/contraction as well as cure shrinkage.

(2)

Here, $_k$ c^2 s^2 $2cs$ s^2 c^2 $2cs$ cs cs c^2 s^2 , c cos and s sin (3)

The temperature-dependent elastic compliance matrix $S\ T$, which is the inverse of the stiffness matrix, can be calculated using the temperature-dependent material properties $E_L\ T$ $E_T\ T$ obtained from DMA, the manufacturer provided Poisson s ratio of 0.35 and in-plane shear modulus of 5 GPa through Eq. (4). While the material is expected to exhibit linear-elasticity for small strains after vitrification, this behavior is also assumed before vitrification from the stress-free point. This assumption enables the computation of a rough magnitude of residual stress during the hold phase. From the compliance matrix, the stiffness matrix is simply calculated as Q S ^{1}.

(4)

The residual stress for each ply is calculated using the residual strain determined from Eq. (2) and the temperature-dependent stiffness matrix [Q] of the composite panel as shown in Eq. (5). The continuous evolution of this residual stress in each ply for all sample configurations can be seen in Figs. 8-13.

(5)

The residual stresses are calculated using Eq. (5) for all the layup configurations used in this research and are plotted in Figs. 8-13. For [0/90]$_s$ configuration, the change in residual stress is less during the hold-phase until the vitrification point and then rapidly increases to a maximum of 110 MPa and 24.21 MPa in longitudinal and transverse directions for 0 ply as seen in Fig. 8. This is the highest residual stress observed among the current ply configurations in the longitudinal direction due to the cross-ply nature of the layup. It can also be observed that the highest residual stress for 0 ply is in the longitudinal direction and for 90 ply it is observed in the transverse direction as the fibers in these respective (parallel-to-the-fibers) directions have high modulus and low thermal expansion coefficient giving rise to the macro stresses during the cool-down [8].

The residual stresses in [0/45]$_s$ along with the rest of the layup configurations follow a similar trend to [0/90]$_s$ changing rapidly after vitrification during the cool-down phase. In the longitudinal direction, 0 ply exhibited compressive stress of 47 MPa, and 45 ply has residual stress of 138 MPa at the end of the cure. In the transverse direction, they exhibit 6.5 MPa and 14.5 MPa respectively. The rate of change in longitudinal residual stress is higher in 45 ply at vitrification compared to 0 ply. This particular difference can only be observed through the continuous evolution of residual stresses as shown in Fig. 9. In the case of anti-symmetric angle-ply [45/ 45/45/ 45] configuration, as seen in Fig. 10, 45 ply and 45 ply exhibit similar stresses in both longitudinal and transverse direction. The coordinate transformation in the stress calculations for this layup resulted in a wider range for the error bars. Note that the error bars for the corresponding longitudinal strain measurements in Fig. 6 are relatively low.

For balanced unsymmetrical [30/ 30/60/ 60] layup configuration, it can be observed from Fig. 11 that in the longitudinal direction the plies exhibited compressive stresses and in the transverse direction,

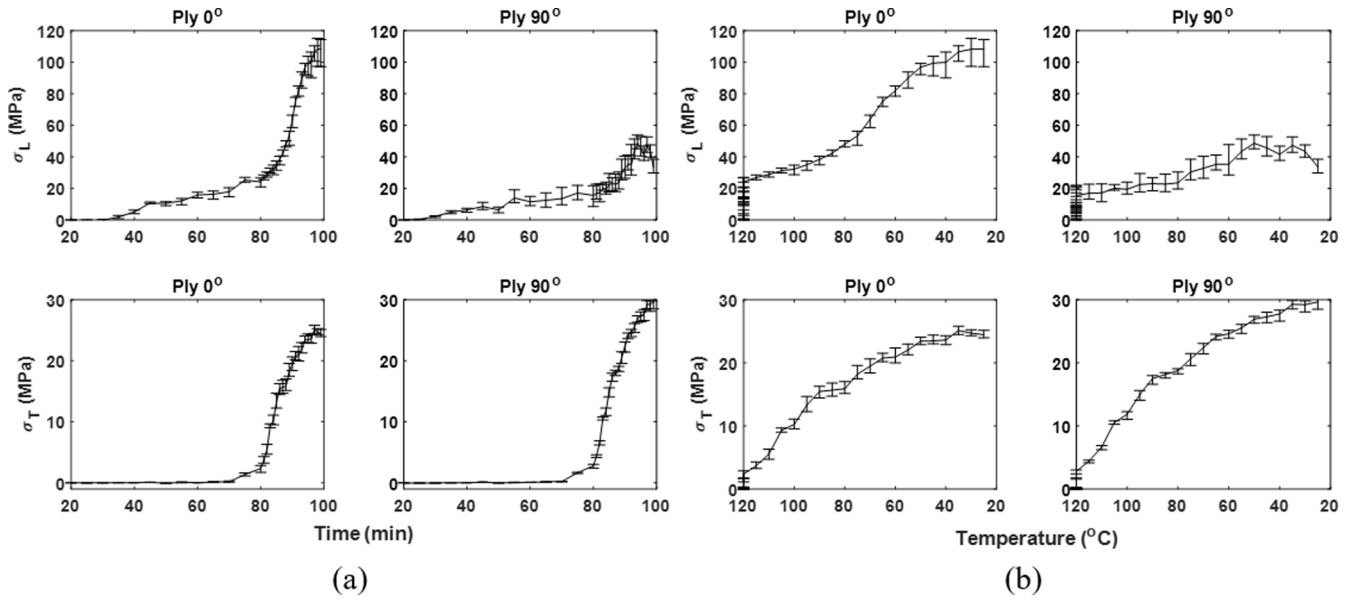

Fig. 8. Ply stresses in $[0/90]_s$ laminate for the plies oriented in 0 and 90 : (a) plotted against time; (b) plotted against temperature.

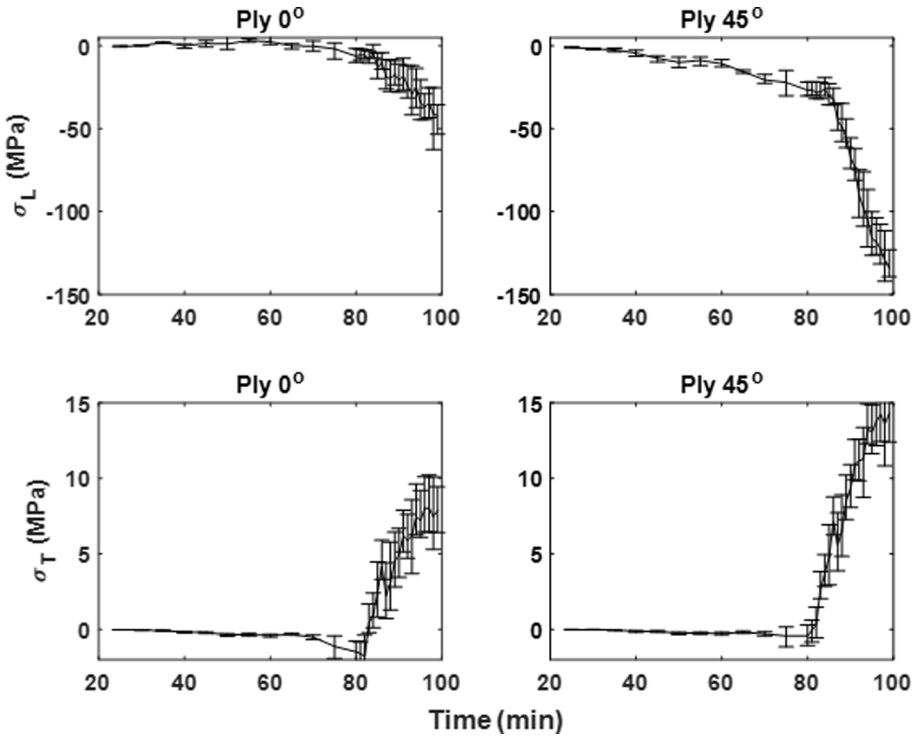

Fig. 9. Ply stresses in $[0/45]_s$ laminate for the plies oriented in 0 and 45°.

they are in tension. The rate of evolution of stresses in the longitudinal direction during the hold phase is higher for 60 ply followed by 30 ply, 30 ply, and 60 ply. The ability of 60 to relax stresses during the cool-down phase is restricted by the 30 ply and 60 ply on top and bottom respectively. The in-situ ability of the current research approach to calculate the residual stress evolution of the internal plies can be clearly observed here. At the end of the cure, 30 ply has maximum longitudinal compressive stress of 71 MPa followed by 60 ply and 30 ply at 65 MPa and 44.5 MPa respectively. The lowest stress is exhibited by 60 ply. In the transverse direction, relatively smaller changes in the evolution of stresses are observed in all four plies in tension. The highest stress of 13.7 MPa was observed for the 60 ply and the lowest stress of 9.7 MPa for the 60 ply.

In the unsymmetrical [0/30/45/90] layup, while the 0 top ply exhibited 41 MPa stress in tension, both 45 ply and 30 ply exhibit an increase in the rate of compressive residual stress during the hold phase and reached maximum longitudinal compressive stress of 53 MPa and 41 MPa respectively at the end of the cure. The highest longitudinal compressive stress of 132 MPa is observed in 90 ply. This ply also exhibits the highest stress of 17.9 MPa in the transverse direction. As seen in Fig. 12, the rate of change in residual stresses is low during the hold phase until vitrification followed by a rapid increase after vitrification. A similar trend can be observed for all the layups adopted in this research except some plies are in tension and others are in compression.

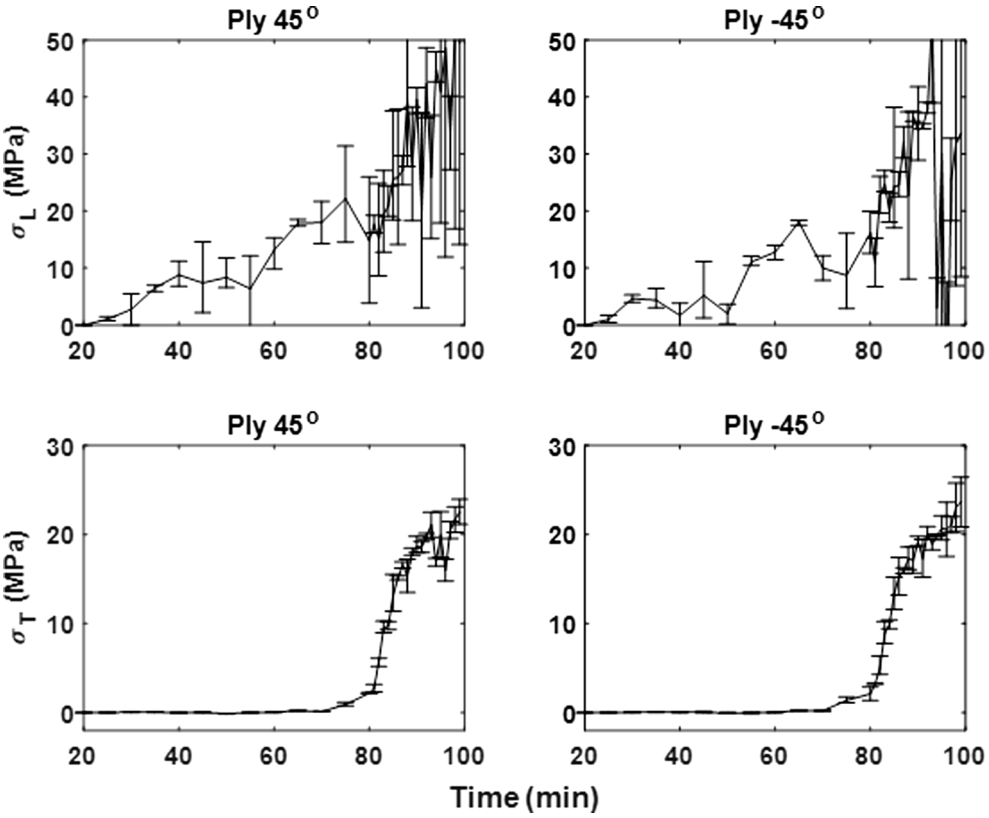

Fig. 10. Ply stresses in [45/ 45/45/ 45] laminate for the plies oriented in 45 and 45°.

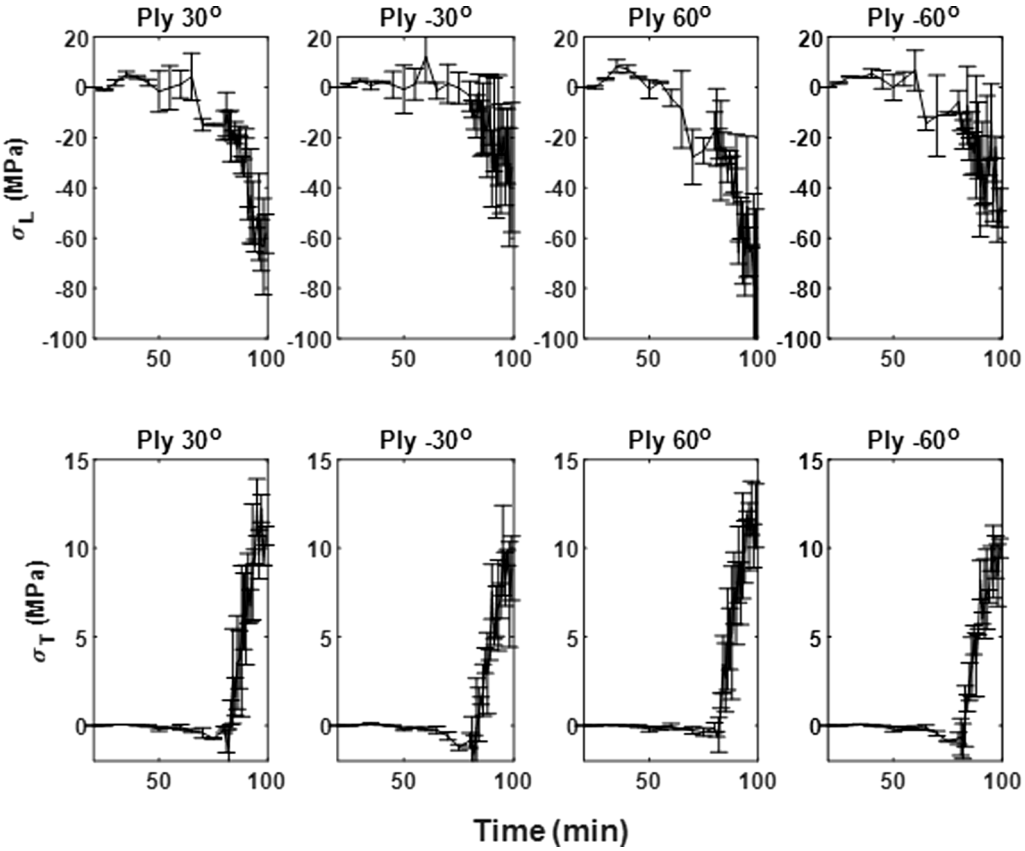

Fig. 11. Ply stresses in [30/ 30/60/ 60] laminate for the plies in respective orientation.

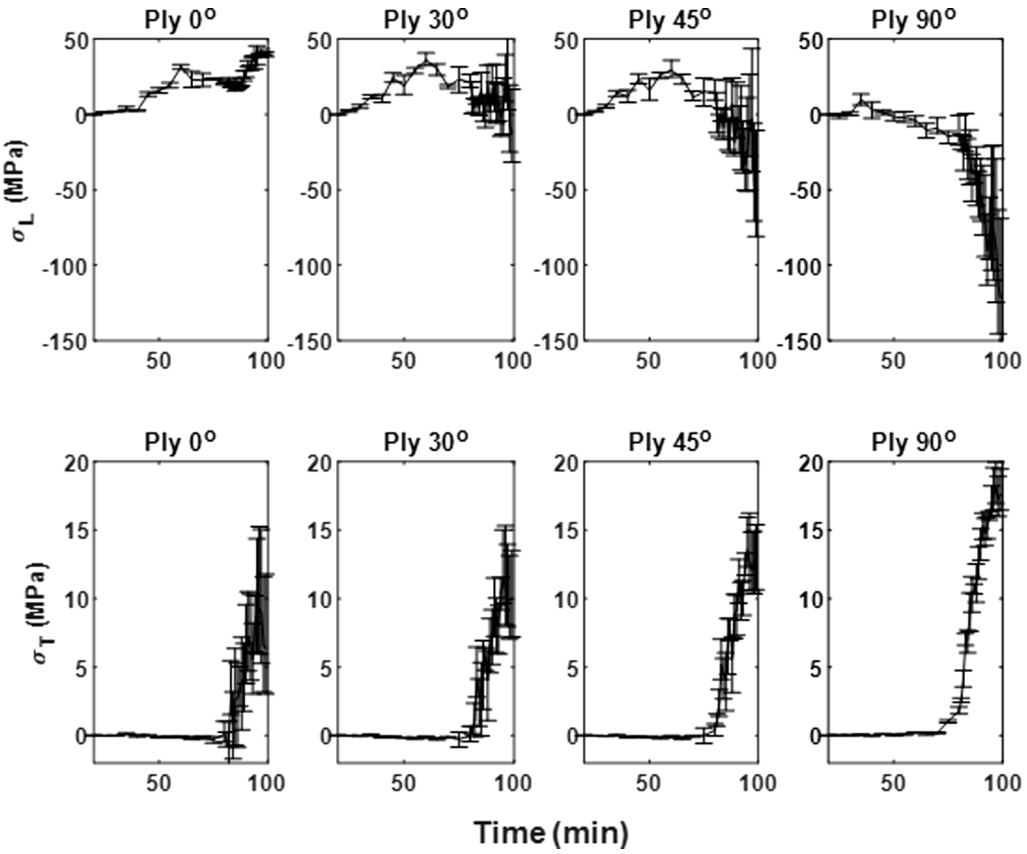

Fig. 12. Ply stresses in [0/30/45/90] laminate for the plies in respective orientation.

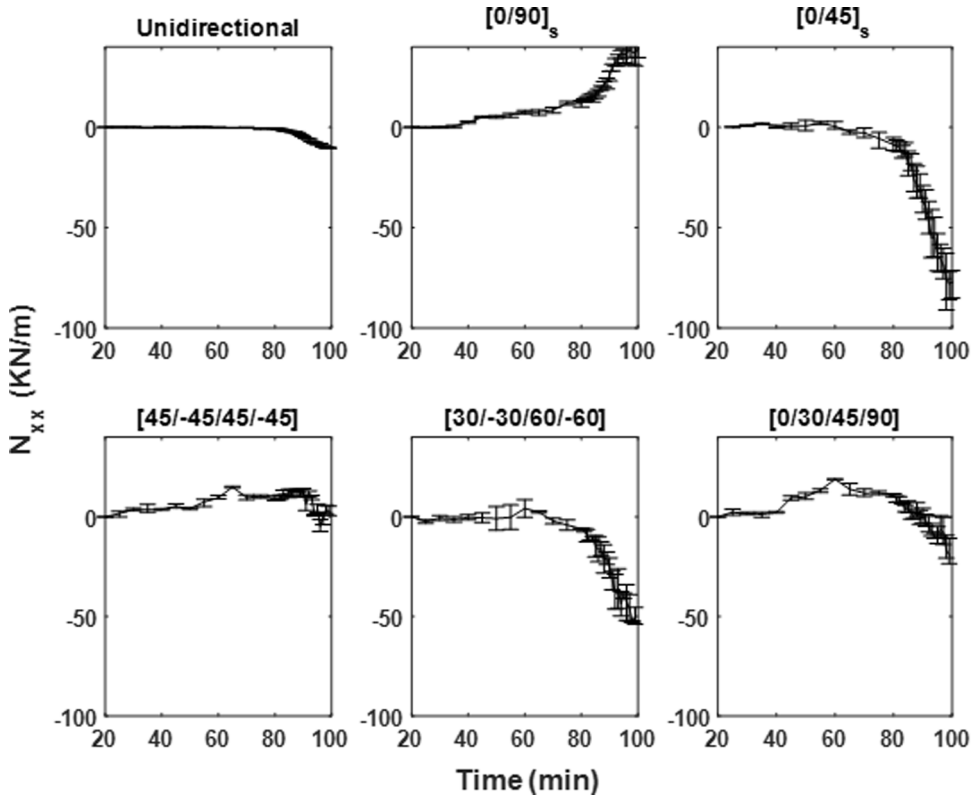

Fig. 13. Laminate normal forces (N_{xx}).

The cross-ply $[0/90]_s$ layup exhibits the highest residual stress, followed by the rest of the layup configurations. The amount of stress buildup during the hold and cool-down phase directly corresponds to the strain evolution of that particular layup and associated ply stiffness. For example, in the case of $[0/90]_s$ laminate, there is stress buildup in both 0 and 90 plies in the longitudinal direction but not in the transverse direction. This is because the strain during the isothermal stage in the longitudinal direction is higher than in the transverse direction for $[0/90]_s$ laminate (as seen in Figs. 6 and 7).

It is to be noted that the DIC surface strain measurements are made in autoclave conditions i.e. under continuous vacuum and pressure. Hence the stresses measured are also under the same autoclave conditions. When the laminates are removed from the autoclave after cure, residual stresses in certain asymmetric layups are relaxed by developing the warpage. The effect of the warpage is discussed in section 3.6.

3.5. Laminate normal forces and moments

In this section, the evolution of laminate forces and moments are calculated using the laminate strains obtained from DIC and the temperature-dependent stiffness matrix [*Q*]. The Classical Lamination Theory (CLT) approach [32] based on the ABD matrix as shown in Eq. (6) is used for calculating the forces and moments. Here, the strains are under autoclave conditions of vacuum and pressure, and the laminate does not exhibit curvature ( ) under these conditions. Once the laminate is removed from the autoclave, the residual moments at the end of the cure cause warpage in the asymmetric layups.

(6)

The continuous evolution of normal forces N_{xx} and N_{yy} in the laminate are plotted for all sample configurations in Figs. 13 and 14 respectively. The evolution of moments for asymmetric layups are plotted in Fig. 15. While residual stresses in a laminate are per ply, these normal forces and moments provide an overall effect of those residual stresses on the specimen. Comparing the evolution of residual stresses and laminate normal forces, both follow similar trends for a given layup. It can be seen in Fig. 13 that the normal force (N_{xx}) for cross-ply $[0/90]_s$ layup is in tension and the rest of the layup configurations are in compression. Similarly from Fig. 14, it can be observed that a maximum compressive normal force (N_{yy}) of 55 KN/m is observed for balanced [30/ 30/60/ 60] layup and the lowest compressive normal force of approx. 0 KN/m is observed for unidirectional single-ply lamina.

The evolution of moments for asymmetric layups can be seen in Fig. 15. It can be observed that the maximum overall moment at the end of the cure is observed for balanced unsymmetric [30/ 30/60/ 60] layup followed by [45/ 45/45/ 45] layup and [0/30/45/90]. This agrees with the warpage calculations performed on the laminate after removing it from the autoclave vacuum and pressure as seen in Table 1.

3.6. Discussion

Residual stresses in carbon fiber composites arise during the manufacturing process due to the thermal and chemical properties of the material. Thermal residual stresses are primarily due to differential CTE when the material is heated and the chemical stresses are due to the matrix shrinkage during cure. The matrix is viscous until it reaches the gel point which is ~ 120 C for the prepreg used in this research and becomes rubbery after gelation [24]. This is also the point of stress-free temperature where the internal stresses present in the material are liberated [33]. For the manufacturer specified cure cycle, this stress-free point is achieved at 20 min into the cure, and the vitrification point occurs at 70 min into the cure as shown in Fig. 4. The combination of the glassy matrix after vitrification and the thermal relaxation of the matrix and fibers during the cool-down phase creates residual stresses when the laminate is cooled to ambient temperatures. This can be observed in the continuous evolution of stresses analyzed in this research.

Unbalanced residual stresses in asymmetric layups are relaxed by

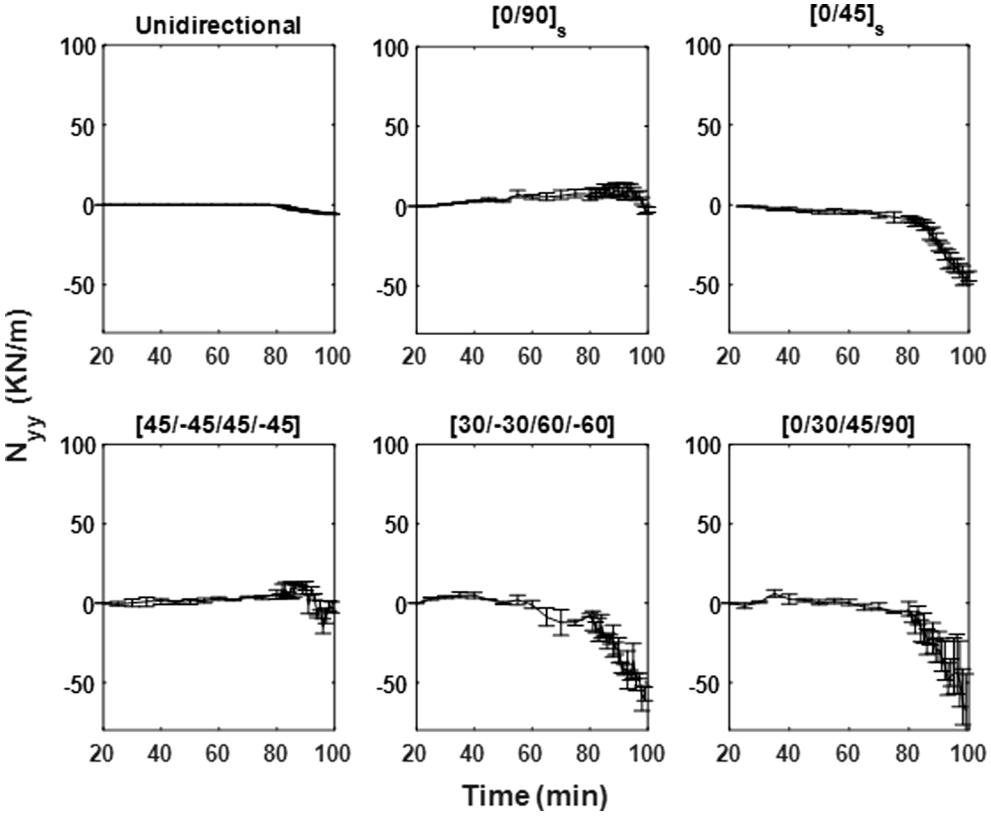

Fig. 14. Laminate normal forces (N_{yy}).

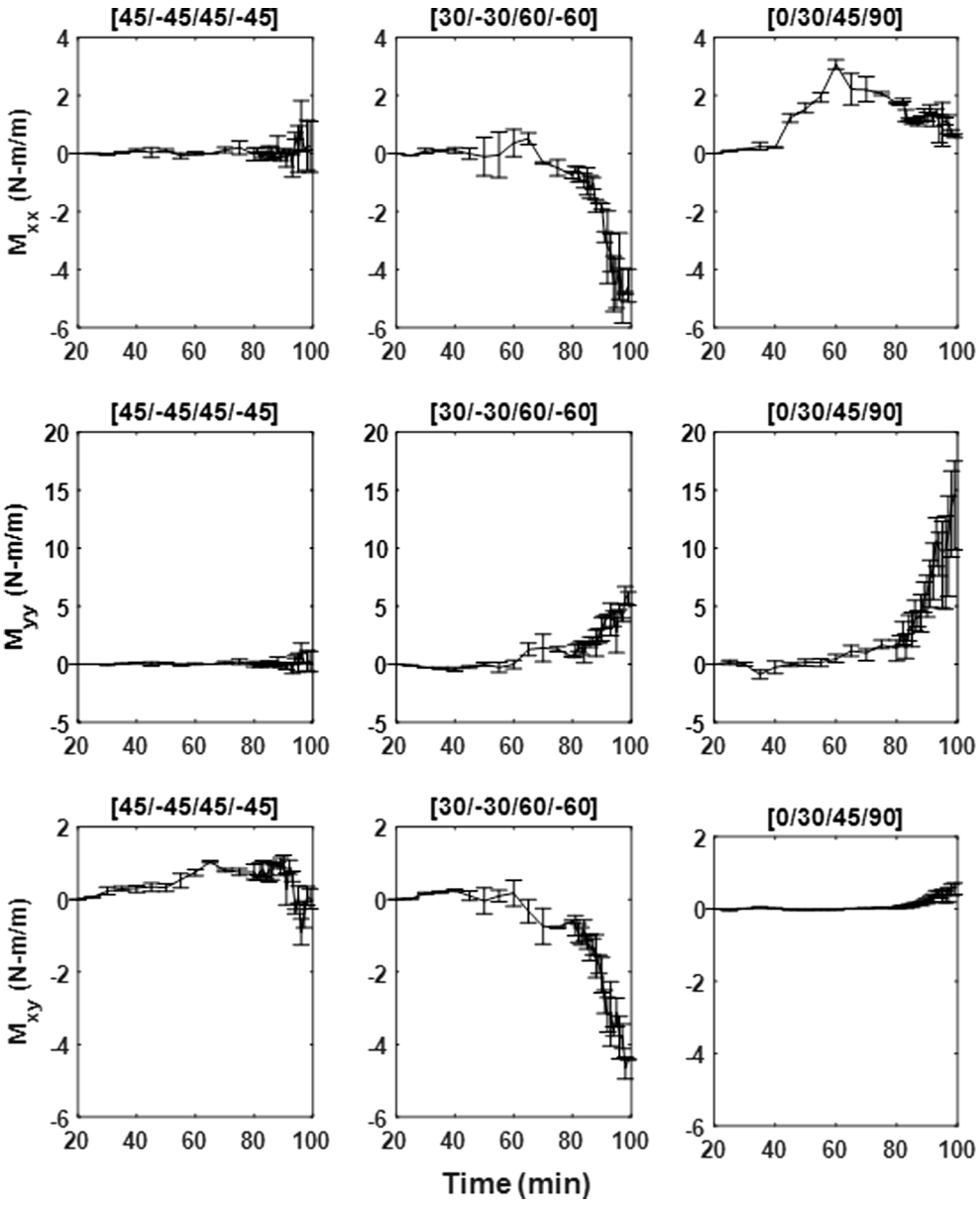

Fig. 15. Laminate moments for all asymmetric layups.

Table 1
Average cup, bow, and twist measurements for asymmetric layups.

Configurations	Cup (mm)	Bow (mm)	Twist (mm)	Total Warp (mm)
[45/ 45/45/ 45]	0	0	0.83	0.83
[30/ 30/60/ 60]	0.23	0.6	0.63	1.46
[0/30/45/90]	0.53	0	0.18	0.71

creating a warpage in the laminate after processing. Numerous researchers calculated the residual stresses using the warpage developed in asymmetrical laminates at the end of the cure using CLT. Wisnom et al. measured temperature-related change in curvature to study residual stresses in asymmetric laminates [4]. They observed that curvature due to the residual stresses develop during cool-down after vitrification. Jain et al. analyzed the curvature of structural components to estimate residual stresses using modified shell theory [34]. These methods of calculating residual stresses cannot be applied to symmetric laminates due to their inability to develop curvature or warpage. A destructive method is adopted to calculate residual stresses in symmetric laminates by milling layers from one side of the laminate to relieve the residual stresses, thus producing a warped laminate [8]. The measured curvature after milling and CLT are used to calculate the residual stresses. The current method of calculating residual stresses is not only non-destructive but also gives the evolution of the residual stresses throughout the cure for both symmetric and asymmetric laminates. The DIC strain measurements obtained in this research are under autoclave conditions of vacuum and pressure, hence the residual stresses calculated in this research are the actual stresses in the laminates under vacuum bagging. In asymmetric laminates, some of these residual stresses will be relaxed to create a warpage after processing.

Warpage in flat laminates is calculated as a combination of cup, bow, and twist deviations from its initial flatness as shown in Fig. 16. The angle ply nature of [45/ 45/45/ 45] layup contributes only to twist without any cup or bow warp. In the case of balanced [30/ 30/60/ 60] layup, while the difference in alternating orientations of 30 and 60 plies creates bow, the angled ply layup leads to the twist deformation. The combination of both bow and twist in this balanced

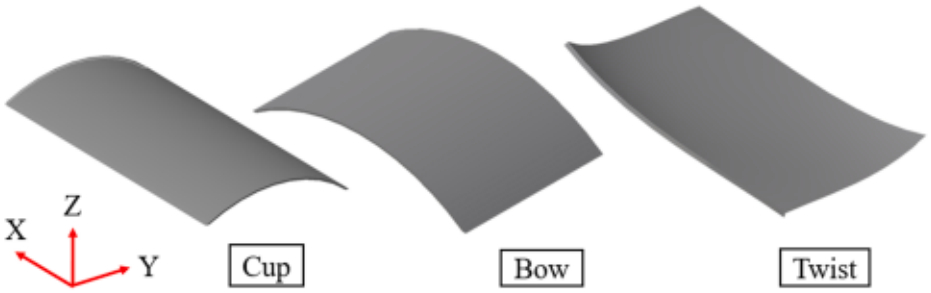

Fig. 16. Warpage shown as cup, bow, and twist of the laminate.

layup creates small cup warpage. The absence of any negative direction ply eliminates bow warp in [0/30/45/90] layup. While the 30° and 45° plies in the middle contribute to twist, the 0° and 90° plies on top and bottom contribute to the cupping effect. The average warpage for the asymmetric layup configurations adopted in this research can be seen in the table (1). Comparing table (1) and residual moments in Fig. 15, it is clear that the relaxation of residual moments leads to warpage in asymmetric layups after removing from vacuum conditions.

3.7. Conclusion

The growing use of advanced composite laminates in recent years has focused attention on processing-induced defects such as delaminations and matrix cracking which are caused by residual stresses. In the current work, the continuous evolution of residual stresses during composite processing is investigated by combining the dimensional changes measured using a novel in-situ experimental approach with temperature-dependent moduli obtained from DMA. The main research findings are summarized below:

a. The experimental approach developed in this research is effective in calculating the residual stresses throughout the cure for both symmetric and asymmetric layups. The pattern of residual stresses developed after curing in all the layup configurations correlates with knowledge from literature.
b. The combination of strain evolution and increase in modulus during cool down lead to a rapid increase in the residual stresses after vitrification. This is observed for all the layups considered in this research.
c. Among the symmetric layups, $[0/90]_s$ cross-ply layup exhibited maximum residual stress of 110 MPa in the longitudinal direction followed by $[0/45]_s$.
d. Among the asymmetric layups, balanced unsymmetric [30/−30/60/−60] layup exhibited maximum residual stress followed by [45/−45/45/−45] and [0/30/45/90] layups.
e. Warpage is developed in all three asymmetrical layups after processing. Higher residual stresses resulted in higher average warpage with the balanced unsymmetric [30/−30/60/−60] layup exhibiting an average warp of 1.46 mm.

CRediT authorship contribution statement

Sandeep Chava: Conceptualization, Investigation, Methodology, Validation, Visualization, Writing - original draft, Writing - review & editing. **Sirish Namilae:** Conceptualization, Investigation, Methodology, Validation, Supervision, Funding acquisition, Writing - review & editing.

Declaration of Competing Interest

None.

Acknowledgment

The authors would like to acknowledge Dr. Sandra Boetcher and Dr. Marwan Al-Haik for their support in using the DSC and DMA machines. We thank the two anonymous reviewers whose comments/suggestions helped improve and clarify this manuscript. This research was supported by NSF Advanced Manufacturing grant number 2001038.

References

[1] Cheng W, Finnie I. Residual Stress Measurement and the Slitting Method. Springer Science & Business Media; 2007. https://doi.org/10.1007/978-0-387-39030-7.
[2] LIU S-C. Residual stress characterization for laminated composites 1999:169.
[3] Klingbeil NW, Beuth JL, Chin RK, Amon CH. Residual stress-induced warping in direct metal solid freeform fabrication. Int J Mech Sci 2002;44:57–77. https://doi.org/10.1016/S0020-7403(01)00084-4.
[4] Wisnom MR, Gigliotti M, Ersoy N, Campbell M, Potter KD. Mechanisms generating residual stresses and distortion during manufacture of polymer-matrix composite structures. Compos Part A Appl Sci Manuf 2006;37:522–9. https://doi.org/10.1016/j.compositesa.2005.05.019.
[5] Chiang MYM, McKenna GB, Yuan J. A viscoelastic micor-mechanical analysis for dimensional stability of a composite layer. Polym Eng Sci 1994;34:1815–22. https://doi.org/10.1002/pen.760342406.
[6] Nairn JA. Matrix Microcracking in Composites. Compr Compos Mater 2000;2:403–32. https://doi.org/10.1016/b0-08-042993-9/00069-3.
[7] Chapman TJ, Gillespie JW, Pipes RB, Manson JAE, Seferis JC. Prediction of process-induced residual stresses in thermoplastic composites. J Compos Mater 1990;24:616–43. https://doi.org/10.1177/002199839002400603.
[8] Cowley KD, Beaumont PWR. The measurement and prediction of residual stresses in carbon-fibre/polymer composites. Compos Sci Technol 1997;57:1445–55. https://doi.org/10.1016/S0266-3538(97)00048-1.
[9] Wu Z, Lu J, Han B. Study of residual stress distribution by a combined method of moir interferometry and incremental hole drilling, part II: Implementation. J Appl Mech Trans ASME 1998;65:844–50. https://doi.org/10.1115/1.2791920.
[10] Hannuach S, Stockmann M, Ihlemann J. Experimental Method for Residual Stress Analysis with Fibre Bragg Grating Sensors. Mater Today Proc 2016;3:979–82. https://doi.org/10.1016/j.matpr.2016.03.032.
[11] Jeronimidis G, Parkyn AT. Residual stresses in carbon fibre-thermoplastic matrix laminates. J Compos Mater 1988;22:401–15. https://doi.org/10.1177/002199838802200502.
[12] Pintschovius L. Determination of residual stresses by neutron diffraction. Mem Etudes Sci La Rev Metall 1989;86:723–8. https://doi.org/10.1016/s0026-0657(96)93572-9.
[13] Stacey A, Webster PJ, Ziebeck KRA. Measurement of residual stresses by neutron diffraction. J Strain Anal Eng Des 1985;20:93–100. https://doi.org/10.1243/03093247V202093.
[14] Pawlak A, Zinck P, Galeski A, Gerard JF. Photoelastic studies of residual stresses around fillers embedded in an epoxy matrix. Macromol. Symp., vol. 169, Wiley Online Library; 2001, p. 197–210. https://doi.org/10.1002/1521-3900(200105)169:1<197::AID-MASY197>3.0.CO;2-2.
[15] Wenzelburger M, López D, Gadow R. Methods and application of residual stress analysis on thermally sprayed coatings and layer composites. Surf Coat Technol 2006;201:1995–2001. https://doi.org/10.1016/j.surfcoat.2006.04.040.
[16] Jannotti P, Subhash G, Zheng J, Halls V. Measurement of microscale residual stresses in multi-phase ceramic composites using Raman spectroscopy. Acta Mater 2017;129:482–91. https://doi.org/10.1016/j.actamat.2017.03.015.
[17] Kandil Fa, Lord JD, Fry aT, Grant PV. A review of residual stress measurement methods - A guide to technical selection. NPL Mater Cent 2001;1–42.
[18] Ifju PG, Niu X, Kilday BC, Liu SC, Ettinger SM. Residual strain measurement in composites using the cure-referencing method. Exp Mech 2000;40:22–30. https://doi.org/10.1007/BF02327544.
[19] Croom BP, Bumgardner C, Li X. Unveiling residual stresses in air plasma spray coatings by digital image correlation. Extrem Mech Lett 2016;7:126–35. https://doi.org/10.1016/j.eml.2016.02.013.
[20] Wu AS, Brown DW, Kumar M, Gallegos GF, King WE. An Experimental Investigation into Additive Manufacturing-Induced Residual Stresses in 316L

Stainless Steel. Metall Mater Trans A Phys Metall Mater Sci 2014;45:6260 70. https://doi.org/10.1007/s11661-014-2549-x.
[21] Safarabadi M. Evaluation of curing residual stresses in three-phase thin composite laminates considering micro-scale effects. J Compos Mater 2016;50:3753 64. https://doi.org/10.1177/0021998315624252.
[22] Huang ZM. Strength formulae of unidirectional composites including thermal residual stresses. Mater Lett 2000;43:36 42. https://doi.org/10.1016/S0167-577X(99)00227-X.
[23] Jin KK, Huang Y, Lee YH, Ha SK. Distribution of micro stresses and interfacial tractions in unidirectional composites. J Compos Mater 2008;42:1825 49. https://doi.org/10.1177/0021998308093909.
[24] Chava S, Namilae S. In-situ investigation of the kinematics of ply interfaces during composite manufacturing. J Manuf Sci Eng 2020:1 28. https://doi.org/10.1115/1.4047740.
[25] Prepreg Unidirectional Carbon Fiber Fabric n.d. https://www.fibreglast.com/category/PrePreg_Fabrics (accessed March 5, 2020).
[26] Li F, Leng J, Liu Y, Remillat C, Scarpa F. Temperature dependence of elastic constants in unidirectional carbon fiber reinforced shape memory polymer composites. Mech Mater 2020;148:103518. https://doi.org/10.1016/j.mechmat.2020.103518.
[27] Kim KS, Hahn HT. Residual stress development during processing of graphite/epoxy composites. Compos Sci Technol 1989;36:121 32. https://doi.org/10.1016/0266-3538(89)90083-3.
[28] Hardis R, Jessop JLP, Peters FE, Kessler MR. Cure kinetics characterization and monitoring of an epoxy resin using DSC, Raman spectroscopy, and DEA. Compos Part A Appl Sci Manuf 2013;49:100 8. https://doi.org/10.1016/j.compositesa.2013.01.021.
[29] Montserrat S. Vitrification and further structural relaxation in the isothermal curing of an epoxy resin. J Appl Polym Sci 1992;44:545 54. https://doi.org/10.1002/app.1992.070440319.
[30] Correlated Solutions DIC System Specifications n.d. https://www.correlatedsolutions.com/vic-3d/ (accessed January 14, 2021).
[31] Thai TQ, Hansen RS, Smith AJ, Lambros J, Berke RB. Importance of exposure time on DIC measurement uncertainty at extreme temperatures. Exp Tech 2019;43:261 71.
[32] Jones RM. Mechanics of composite materials. CRC Press; 1998.
[33] Pethrick RA. Bond Inspection in Composite Structures. Compr Compos Mater 2000;359 92. https://doi.org/10.1016/b0-08-042993-9/00080-2.
[34] Jain LK, Mai YW. On residual stress induced distortions during fabrication of composite shells. J Reinf Plast Compos 1996;15:793 805. https://doi.org/10.1177/073168449601500803.